

# Exploring MSSM for charge and color breaking and other constraints in the context of Higgs@125 GeV.

---

**Utpal Chattopadhyay, Abhishek Dey**

*Department of Theoretical Physics, Indian Association for the Cultivation of Science, 2A & B Raja S.C. Mullick Road, Jadavpur, Kolkata 700 032, India*

*E-mail:* [tpuc@iacs.res.in](mailto:tpuc@iacs.res.in), [tpad4@iacs.res.in](mailto:tpad4@iacs.res.in)

**ABSTRACT:** Exploring MSSM parameter space after the discovery of Higgs Boson at 125 GeV naturally demands large top-squark mixing or large trilinear coupling parameter  $A_t$  in particular, so as to avoid excessively heavy squark, specially for the universal models like CMSSM. We study stability of electroweak symmetry breaking vacua in possible presence of deeper charge-color symmetry breaking minima within MSSM. Besides stable vacua, we consider scenarios characterized by the presence of global CCB minima, with SM like charge and color conserving vacuum, having stability over cosmologically large lifetime (*long-lived states*). We allow vacuum expectation values for both stop as well as sbottom fields, since these belong to the third generation of sfermions with larger Yukawa couplings that have immediate effect on the tunneling time. Moreover, for large  $\mu$  regions, radiative corrections to Higgs boson mass from bottom-squark loop is quite significant. Regions of MSSM parameters space become viable for large  $A_t$  and large  $\mu$  zones which are generically excluded via the traditional analytical CCB constraints. For a large value of  $\tan \beta$ , safe vacua associated with large values of  $|\mu|$  and  $|A_t|$  are predominantly long-lived and may be associated with relatively light stop masses. We also identify low  $\mu$  regions associated with long-lived states. Both the above zones can be friendly to muon  $g - 2$  constraint. We also impose constraints from  $\text{Br}(B \rightarrow X_s \gamma)$  and  $\text{Br}(B_s \rightarrow \mu^+ \mu^-)$ . We do the analysis for a moderate and a large  $\tan \beta$ . We choose an example parameter point in the gaugino mass plane of  $M_1, M_2$  that satisfies the dark matter constraints, basically a decoupled sector with respect to CCB.

---

## Contents

<b>1</b>	<b>Introduction</b>	<b>1</b>
<b>2</b>	<b>Aspects of CCB minima, Decay of False Vacuum and MSSM</b>	<b>3</b>
<b>3</b>	<b>Results</b>	<b>7</b>
3.1	Study of generic region of pMSSM parameter space for the stability of vacuum	7
3.2	Stability of vacuum for a fixed $\tan\beta$ and a large $ \mu $	9
3.3	Scan over wide range of $\mu$ and $A_t$ for $\tan\beta = 20$	11
3.3.1	Maximized $m_h$ zones in relation to long-lived states: Regions I and II	12
3.3.2	Compatibility with dark matter related constraints	14
3.4	Scan over wide range of $\mu$ and $A_t$ for $\tan\beta = 40$	16
3.5	Muon $g - 2$	21
<b>4</b>	<b>Conclusion</b>	<b>22</b>
<b>5</b>	<b>Acknowledgment</b>	<b>24</b>

---

## 1 Introduction

In the Standard Model (SM)[1] of Particle Physics the electrically neutral component of the electroweak scalar doublet (Higgs) takes a non-zero vacuum expectation value ( $vev$ ) in the ground state leading to spontaneous symmetry breaking (SSB). This leads to generation of mass of  $SU(2)_L$  gauge bosons and mass for fermions through Yukawa terms. Lorentz invariance of the vacuum prevents any object other than a Lorentz scalar from acquiring a non-zero  $vev$ . The only scalar present in SM is the Higgs scalar which is singlet under  $SU(3)$  color ( $SU(3)_C$ ). The presence of physically equivalent continuum of degenerate minima in SM Higgs potential, enables one to define the unbroken  $U(1)$  generator as the electric charge. This along with unbroken  $SU(3)_C$  leads to charge and color conservation for the ground state of SM, where the Higgs field acquires a non-vanishing  $vev$ . Supersymmetry (SUSY) that can potentially ameliorate the hierarchy problem associated with SM is one of the most viable candidates for Beyond the Standard Model (BSM) physics [2–5]. In the simplest SUSY extension of SM, namely the Minimal Supersymmetric Standard Model (MSSM)[2–6], SM fermions and bosons are supplemented by bosonic and fermionic partners transforming under the same SM gauge group  $SU(3)_C \times SU(2)_L \times U(1)_Y$ . Thus there are new scalars like squarks ( $\tilde{q}$ ) and sleptons ( $\tilde{l}$ ) that are charged under  $SU(3)_C$  and  $U(1)_{EM}$ . The full MSSM scalar potential may indeed have several minima where squarks or sleptons may additionally acquire non-zero  $vevs$ .

Since the violation of charge and/or color quantum number is yet to be observed, it is understood that the Universe at present is at a ground state which is Standard Model like (SML), with only Higgs scalars acquiring *vevs*. *A priori* it indicates that those parts of the multi-dimensional parameter space corresponding to MSSM scalar potential that allow a deeper charge and color breaking (CCB) minima[7–15] should be excluded. This puts severe constraints on the parameter space. However, truly there is no reason to assume that the present SML minima where the Universe rests is a true vacuum. The Universe, in principle can rest in a local minima/false vacuum, provided the lifetime of this SML minima with respect to the decay time into a deeper CCB minima transition is cosmologically large (larger than the age of the Universe). The Universe is then said to reside in a *long-lived* state[16–20]. Analytically minimizing MSSM potential containing large number of scalar fields is very difficult unless one considers simplifying assumptions. This may even put more stringent constraints than what are actually required [18, 19, 21]. Hence, for a given point in the multi-dimensional parameter space it is important to check the existence of any deeper CCB minima numerically as exhaustively performed in codes like **Vevacious**[22] that in turn uses **CosmoTransitions**[23]. In case such minima exist one should compute the lifetime of the false vacuum and decide on the validity of the given point of parameter space depending on the computed lifetime. A parameter point which would either correspond to a stable or a long-lived vacuum state would be referred to have a safe vacuum.

Since the Higgs boson has been found to have a mass of around 125 GeV [24, 25] which is not very far from the upper limit of MSSM predicted value ( $\sim 135$  GeV), it has become important to explore the phenomenological MSSM (pMSSM)[26] parameter space that may give large radiative corrections to the Higgs boson mass and provides with a relatively lighter top squarks. This may be handled by properly considering the trilinear coupling parameter  $A_t$  and the Higgsino mixing parameter  $\mu$ , both of which may on the other hand be sensitive to the CCB constraints. After the Higgs boson is discovered, analyses have been performed considering the existence of long lived states both in Constrained MSSM (CMSSM) as in Ref.[27] as well as in pMSSM context as worked in Ref.[28–30]. All the above works that probed CCB minima numerically, considered values of  $\mu$  less than a TeV or so while exploring  $A_t$  appropriately via satisfying the requirement of long-lived states and the Higgs mass constraint. In this work we probe the pMSSM parameter space in a wider area of  $\mu - A_t$  plane for specific zones of  $\tan\beta$ , where  $\tan\beta$  is the ratio of Higgs vacuum expectation values, and explore the possibility of long-lived states that would also satisfy phenomenological constraints from  $\text{Br}(B \rightarrow X_s \gamma)$ ,  $\text{Br}(B_s \rightarrow \mu^+ \mu^-)$ , muon  $g - 2$  and dark matter. We will specifically explore the above scenario for large values of  $\tan\beta$  that may have important effect on the existence of long-lived states. We should mention here that both  $\text{Br}(B \rightarrow X_s \gamma)$  and  $\text{Br}(B_s \rightarrow \mu^+ \mu^-)$  may have important characteristics for large  $\mu$ ,  $A_t$  and  $\tan\beta$ . While analyzing large  $\mu$  scenarios we also allow non-vanishing *vevs* for third generation of scalar fields beyond top-squarks. We will additionally highlight the issue of radiative corrections to the Higgs boson mass from the bottom-squark and the tau-slepton sectors for large values of  $\mu \tan\beta$  that could

potentially reduce the mass of Higgs boson while  $\mu$  is increased. Furthermore, as we will see soon, validity of both large and small  $\mu$  regions, with large  $A_t$  may be highly interesting in relation to the muon  $g - 2$  result.

This work which is done using **Vevacious**[22] is organized as follows. In Section 2 we briefly discuss essential theoretical aspects of CCB minima, decay of false vacuum and its theoretical implication on MSSM. In Section 3 we present the results of our analysis as follows. First, we will discuss the results for low values of  $\mu$  showing the conformity with past analyses and extend the work for a given large value of  $\mu$ . Thereafter, within the above section we will show the results of scanning over a wide region of  $\mu - A_t$  plane for a moderate as well as for a large value of  $\tan \beta$ . We also discuss the compatibility of our analysis with relevant low energy constraints like those from B-physics and cosmological constraints from neutralino dark matter[32]. We will further discuss the issue of muon  $g - 2$  in the context of long-lived vacuum scenario, presenting also a few benchmark points. Finally, we will conclude in Section-4.

## 2 Aspects of CCB minima, Decay of False Vacuum and MSSM

The MSSM scalar sector consists of squarks and the sleptons and two Higgs doublets with opposite  $U(1)_Y$  hypercharge. The sfermions, charged under  $SU(3)_C \times SU(2)_L \times U(1)_Y$  may acquire non-zero *vevs*. This may result into the existence of potentially dangerous CCB minima that may lie below an SML vacuum. The rate of tunneling from SML false vacuum to such CCB true vacuum is roughly proportional to  $e^{-a/y^2}$ , where  $a$  is a constant and  $y$  is the Yukawa coupling, signifying a larger decay rate for enhanced Yukawa coupling[8, 18, 19]. Hence the third generation of sfermions will be the most important candidate in connection with the formation of potentially dangerous global minima. We do not consider the direction where a sneutrino  $\tilde{\nu}$  may acquire a *vev*, since the corresponding vacuum would conserve both charge and color. In this analysis we would limit ourselves on scenarios where only third generation of squarks may acquire *vevs*.

For simplicity, we now focus on the stop and Higgs fields of the MSSM scalar potential [2–5].

$$\begin{aligned}
V = & (m_{H_u}^2 + \mu^2) |H_u|^2 + (m_{H_d}^2 + \mu^2) |H_d|^2 + m_{\tilde{t}_L}^2 |\tilde{t}_L|^2 + m_{\tilde{t}_R}^2 |\tilde{t}_R|^2 - \\
& B_\mu (H_u H_d + \text{c.c.}) + (y_t A_t H_u \tilde{t}_L \tilde{t}_R + \text{c.c.}) - (y_t \mu \tilde{t}_L \tilde{t}_R H_d^* + \text{c.c.}) + \\
& y_t^2 (|\tilde{t}_L \tilde{t}_R|^2 + |H_u \tilde{t}_L|^2 + |H_u \tilde{t}_R|^2) + \frac{g_2^2}{8} (|H_u|^2 - |H_d|^2 - |\tilde{t}_L|^2)^2 + \\
& \frac{g_1^2}{8} \left( |H_u|^2 - |H_d|^2 + \frac{1}{3} |\tilde{t}_L|^2 - \frac{4}{3} |\tilde{t}_R|^2 \right)^2 + \frac{g_3^2}{6} (|\tilde{t}_L|^2 - |\tilde{t}_R|^2)^2 .
\end{aligned} \tag{2.1}$$

The SML like minima exist in the  $\tilde{t}_L = \tilde{t}_R = 0$  hyperplane, as evident from the above expression. Away from this plane, in the flat direction of quartic terms ( $\tilde{t}_L = \tilde{t}_R$ ), quantities like  $y_t A_t H_u \tilde{t}_R \tilde{t}_L$  and  $y_t \mu \tilde{t}_L \tilde{t}_R H_d^*$  may become large and negative. For large values of  $A_t$  and/or  $\mu$  the above two terms may lead to global minima which break  $U(1)_{\text{EM}}$ ,  $SU(3)_C$  and the global  $U(1)_{\text{Baryon}}$  symmetries. Similar effects occur while *vevs* are considered for  $\tilde{b}_R$ ,  $\tilde{b}_L$  or even for  $\tilde{\tau}_L$  and  $\tilde{\tau}_R$ . Hence it is very

important to probe vacuum stability for large  $|\mu|$  and large A-parameters of third generation in the context of CCB. If the global minima is charge and color breaking, it is essential to evaluate the tunneling rate from SML to CCB minima for estimating the lifetime of the metastable SML state. This lifetime will ultimately determine the viability of the corresponding MSSM parameter point[27–30].

Semiclassical calculations of the false vacuum decay via quantum-tunneling through a barrier, may be performed for a single scalar field  $\phi(\mathbf{x})$  that resulted into the transition probability per unit time per unit volume as given below [18–20].

$$\Gamma/V = Ae^{-S[\bar{\phi}]/\hbar}. \quad (2.2)$$

Here,  $\bar{\phi}$  is a particular configuration of the field  $\phi$  for which  $\delta S=0$ . This field configuration which dominates the integral is called a *bounce*<sup>1</sup>, which is a stationary point of the Euclidean action. The bounce is a non-trivial solution of the Euclidean Euler-Lagrange equation that obeys specific boundary conditions. The probability for the Universe to have decayed to a deeper CCB minima by the present time  $t_0$ , the age of the Universe is roughly equal to  $t_0^4 \times \Gamma/V$ . Here  $t_0^4$  refers to an estimate of a four-volume within which the transition may take place. Considering a 100 GeV scale, thereby  $A \simeq (100 \text{ GeV})^4$ , one obtains  $S_E[\bar{\phi}]/\hbar \sim 400$  for  $t_0^4 \times \Gamma/V \sim 1$ . Therefore, the SML false vacuum at which the Universe rests at the present time may be considered to be stable against decay for  $S_E[\bar{\phi}]/\hbar > 400$ [18, 19], indicating a long-lived scenario. At this point we stress the need of numerical computation. For the simplest case of a single scalar field, explicit analytic calculations may be performed under certain approximations namely the *thin wall* and the *thick wall* scenarios [18–20]. On the other hand, an accurate analysis which involves multiple scalar fields may not divide itself into thin or thick wall zones for phenomenologically significant regions of parameter space. Therefore, one must take resort to numerical computation to determine the fate of SML vacuum in presence of deeper CCB vacua as performed in **Vevacious**[22].

Physics of CCB minima and phase transition in the Early Universe has important implication on the evolution of the Universe and its present ground state [18–20]. As per the previous discussion, the depth of the CCB minima depends on squark/slepton mass terms, the relevant trilinear coupling parameters and  $\mu$ . At a finite temperature the scalar potential is modified by terms  $\propto T^2$  which are similar to mass square terms. The trilinear terms also receive corrections  $\propto T$ . The history of the potential goes as follows[20].

- At a very high temperature, the potential is symmetric with one minima at  $\phi = 0$ .
- Afterwards, at a critical temperature  $T_c$  degenerate minima occur for vanishing as well as non-vanishing  $\phi$ .
- As the temperature decreases with time, the degeneracy breaks and the minima at non-zero  $\phi$  becomes deeper.

---

<sup>1</sup>For details of semiclassical calculation of vacuum decay and related issues see [31].

- Finally, at  $T=0$ , there is a maxima at  $\phi = 0$  and minima at some non-zero  $\phi$  that corresponds to ordinary SML SSB ground state (for  $\phi$  being a neutral colorless scalar).

Transition from an SML minima to a deeper CCB minima which is the focus of our discussion, is a first order phase transition[20].

We shall now discuss the relevance of studying electroweak vacuum stability in the global CCB scenario, in the post Higgs@125 GeV era in which the present data of the Higgs boson mass is  $125.7 \pm 0.6$  GeV [24]. There is a high chance that the discovered Higgs boson is SM like[25]. Hence, in MSSM it would correspond to the CP-even lightest Higgs boson  $h$  assuming a decoupling limit of Higgs scenario ( $M_Z^2 \ll M_A^2$ )[6]. Certainly, with a tree level bound of  $M_Z^2 \cos^2 2\beta$  for  $m_h^2$  one requires a large radiative corrections that on the other hand, push the super-partner spectra on the higher side in unified models. In MSSM this translates to the requirement of heavy top-squarks. The dominant loop correction that is due to the top-stop loops is given by[6]

$$\Delta m_{h,top}^2 = \frac{3g_2^2 \bar{m}_t^4}{8\pi^2 M_W^2} \left[ \ln \left( \frac{m_{\tilde{t}_1} m_{\tilde{t}_2}}{\bar{m}_t^2} \right) + \frac{X_t^2}{m_{\tilde{t}_1} m_{\tilde{t}_2}} \left( 1 - \frac{X_t^2}{12 m_{\tilde{t}_1} m_{\tilde{t}_2}} \right) \right]. \quad (2.3)$$

Here  $X_t = A_t - \mu \cot \beta$  and  $\bar{m}_t$  stands for the running top-quark mass that includes electroweak, QCD and SUSY QCD corrections[33]. With the requirement of the above large loop corrections in the post Higgs discovery scenario, one must explore the regions of parameter space that do not demand so high stop masses but the effect would come from the term involving  $X_t$  in the above equation. The maximal mixing scenario of  $X_t = \sqrt{6}M_S$ , where  $M_S = \sqrt{m_{\tilde{t}_1} m_{\tilde{t}_2}}$  is certainly useful [3–6]. However as we will see in the next section, scenarios of large  $\mu$  are associated with a significant amount of radiative corrections from sbottom and stau loops. As a result, maximal mixing may occur away from  $\sqrt{6}M_S$  for  $X_t$ . We will come to this point soon. While exploring the MSSM parameter space, we must be careful that the MSSM scalar potential may have CCB minima deeper than the SML minima. Therefore, the study of stability of the SML false vacuum against decay to global CCB minima is extremely important. Quite naturally it becomes important to check the degree of effectiveness of the inequalities related to CCB constraints in this regard both for stable and long-lived vacuum states, as we will discuss below.

Suitable analytic constraints were imposed on the relevant MSSM parameters to avoid the appearance of CCB global minima in Refs. <sup>2</sup> [7–14]. The nature of CCB minima and consequently the constraints depend on the particular nature of the *vevs*. In order to derive simpler analytical constraints, assumptions are made depending on the inter-relationships of *vevs* that isolate suitable directions in the field space. In the direction “b” discussed in Ref.[7], non-vanishing *vevs* were considered for  $|H_u|, |H_d|, |Q_u|, |u_R|$  as well as possibly for  $|L_i|$  that under simplifying assumptions of D-flat directions lead to<sup>3</sup>

$$A_u^2 \leq 3[m_2^2 + m_{Q_u}^2 + m_u^2]. \quad (2.4)$$

---

<sup>2</sup>Traditional bounds were initially studied in Refs. 1 and 2 of Ref.[7]. For CCB constraints in models beyond MSSM see Ref.[35]

<sup>3</sup>Following usual notation of fields such as that of Ref.[3].

Here  $m_2^2 = m_{H_u}^2 + \mu^2$ . The above bounds are imposed on all the three generations of up-type squarks and traditionally used in popular SUSY spectrum generators that also use conditions for avoiding potential to be unbounded from below [34]. On the other hand in the direction “a” of Ref.[7] the authors considered non-vanishing  $vevs$  of  $|H_u|, |Q_u|, |u_R|$  as well as that of  $|d_L|, |d_R|$  or possibly  $|L_i|$ , but vanishing  $vev$  of  $|H_d|$  which under simplifying assumptions resulted into the following inequality.

$$A_u^2 \leq 3[m_2^2 - \mu^2 + m_{Q_u}^2 + m_u^2]. \quad (2.5)$$

Using  $m_{H_u}^2 \approx -\mu^2$ , the above reduces to

$$A_u^2 + 3\mu^2 \leq 3[m_{Q_u}^2 + m_u^2]. \quad (2.6)$$

Constraints of Eq.2.6 are valid for small Yukawa couplings. However, if one uses the above for top Yukawa coupling one effectively obtains a stronger bound, embracing the traditional bounds of Eq.2.4 [7]. Going beyond the exact CCB constraints, the possibility of existence of long-lived SML minima were considered afterwards. Thus Ref.[18] and recently Ref.[21] incorporated the above long-lived scenario to come up with the following inequalities that obviously allowed an enlarged parameter space,

$$A_u^2 + 3\mu^2 \leq 7.5[m_{Q_u}^2 + m_u^2], \quad (2.7)$$

$$A_u^2 \leq 3[m_{H_u}^2 + \mu^2] + 7.5[m_{Q_u}^2 + m_u^2]. \quad (2.8)$$

We now try to discuss under what conditions the analytic constraints were evaluated. The simple bounds of Eq.2.4 were obtained considering the D-flat directions assuming  $vevs$  of the concerned scalar fields to be equal. Analysis of realistic scenarios must involve unequal  $vevs$  that is also sufficiently case specific[7]. However, as we will discuss below, even when simplistic assumptions are made for D-flat directions it is seen that more robust bounds such as Eq.2.6 compared to Eq.2.4 may lead to unnecessary degree of stringency[28]. The same is true for the long-lived scenarios of Eq.2.7 and Eq.2.8 which are found to be neither necessary nor sufficient[28–30]. As mentioned previously in this work similar to the Refs.[27–30, 36, 37] we will follow the numerical route to analyze the CCB constraints while considering the possibility of existence of long-lived SML minima. We have used **Vevacious**[22] for our analysis. Combined with a SUSY spectrum generator the code finds the global minima of the associated scalar potential. In absence of global CCB minima the SML vacuum is stable. If the global minima is found to break the charge and color symmetry, the code computes the lifetime of the SML minima against decay to the global CCB minima using the code **CosmoTransitions**[23]. It then determines whether the SML minima is long-lived or short-lived. We will particularly probe the pMSSM parameter space in detail for large  $|\mu|$  and large  $|A_t|$  zones while keeping any issue related to naturalness[38–40] aside. Large  $|\mu|$  is often considered in works involving global analyses of parameter space for unified models like CMSSM[41]. It has also been explored in pMSSM related studies[42] or a similar analysis involving vacuum stability as in Ref.[43].



### 3 Results

Here we present the results of our analysis over different regions of parameter space of pMSSM and classify parameter ranges according to stable, long-lived or short-lived vacua in different subsections. First, we discuss vacuum stability in the generic region of parameter space, in particular for low values of  $\mu$ . Later, we extend our analysis for a large value of  $\mu$  while varying both stop and sbottom sector parameters and assigning *vevs* to stop and sbottom scalar fields. Then we scan over a wide range of values of  $\mu$  and  $A_t$  for a moderate and a large value of  $\tan\beta$  exploring interesting regions of pMSSM parameter space that may potentially fall in the zone of maximal radiative corrections to Higgs boson. This section also analyses the impact of dark matter namely neutralino relic density and direct detection limits on our work. Additionally we will discuss the compatibility of our analysis with muon  $g - 2$  data. The relevant SM parameters used are  $m_t^{pole} = 173.5$  GeV,  $m_b^{MS} = 4.18$  GeV and  $m_\tau = 1.77$  GeV.

#### 3.1 Study of generic region of pMSSM parameter space for the stability of vacuum

In this part we analyze the CCB constraints by focusing on generic part of pMSSM parameter space, in particular for low values of  $\mu$  and non-vanishing  $A_t$  that is important for the Higgs mass limit. Here the parameter space spans a broad range of  $\tan\beta$ , third generation of up-type squark masses,  $A_t$  and  $\mu$  upto a TeV. In this subsection, in order to compare our results with Refs.[28–30] we allow only stop fields ( $\tilde{t}_L$  and  $\tilde{t}_R$ ) to take non-zero *vevs* along with the Higgs fields. Our choice of parameters are as follows.

$$\begin{aligned}
500 \text{ GeV} &\leq m_{\tilde{Q}_3} \leq 1500 \text{ GeV}, \\
500 \text{ GeV} &\leq m_{\tilde{U}_3} \leq 1500 \text{ GeV}, \\
5 &\leq \tan\beta \leq 60, \\
100 \text{ GeV} &\leq \mu \leq 1000 \text{ GeV}, \\
-3 m_{\tilde{Q}_3} &\leq A_t \leq 3 m_{\tilde{Q}_3}.
\end{aligned} \tag{3.1}$$

We set all other sfermion masses to be at 1 TeV,  $M_A = 1$  TeV. The gaugino masses are fixed at  $M_1 = 100$  GeV,  $M_2 = 300$  GeV and  $M_3 = 1000$  GeV. All other trilinear couplings are set to zero. The other sfermion masses or the gaugino masses could indeed be chosen at different zones of values without essentially affecting the results of our analysis involving long-lived states.

Keeping an eye on Eq.2.4 we define  $M_\#^2 = m_{H_2}^2 + \mu^2 + m_{\tilde{t}_L}^2 + m_{\tilde{t}_R}^2$  and plot Fig. 1 for variation of the lightest Higgs boson mass  $m_h$  vs the dimensionless quantity  $A_t^2/M_\#^2$ . This would easily identify our results with respect to the traditional bounds of CCB constraint and additionally show the validity zones of the long-lived states. Blue, green and grey colored points correspond to stable, long-lived and short-lived vacuum states respectively. It is evident from the plot that there exist safe vacua (long-lived and stable states) where the traditional constraint (Eq.2.4) is violated. There is a significant zone of long-lived vacuum states where the Higgs mass is quite high, close to even



the maximum value (see Eq.3.2 and related discussion as given below) a fact generally consistent with the results of Refs.[28–30]. This shows the importance of considering the existence of long-lived states in the post Higgs@125 GeV era. Additionally, even if we do not consider the long-lived states, our numerical exploration of CCB constraints shows that Eq.2.4 is only approximately valid, for example there exist green regions below  $A_t^2/M_{\#}^2 = 3$ .

A similar result when projected into  $m_h$  vs  $X_t/M_S$  plane, (where  $M_S = \sqrt{m_{\tilde{t}_L} m_{\tilde{t}_R}}$ ) appears in Fig. 2. Here  $m_h$  maximizes itself in both the regions, negative and positive for  $X_t$ , where there exist long-lived rather than stable states. We like to mention here that considering the existing uncertainties in the computation of radiative corrections to Higgs mass we assume a 3 GeV window in  $m_h$  leading to the following range[44]. This could arise from renormalization scheme related uncertainties, scale dependence, problems in computing higher order loop corrections up to three loops or the uncertainty in the experimental value of top-quark mass <sup>4</sup>.

$$122 \leq m_h \leq 128 \text{ GeV.} \quad (3.2)$$

We would like to mention that we have imposed the constraints from  $\text{Br}(B \rightarrow X_s \gamma)$  as well as  $\text{Br}(B_s \rightarrow \mu^+ \mu^-)$  in this analysis and the shown parameter points completely satisfy the following conditions irrespective of the nature of the vacuum. The experimental limits on  $\text{Br}(B \rightarrow X_s \gamma)$  as given in [47] is  $\text{Br}(B \rightarrow X_s \gamma) = [3.42 \pm 0.22] \times 10^{-4}$  which at  $3\sigma$  level results into

$$2.77 \times 10^{-4} \leq \text{Br}(B \rightarrow X_s \gamma) \leq 4.09 \times 10^{-4}. \quad (3.3)$$

The recent constraints from  $\text{Br}(B_s \rightarrow \mu^+ \mu^-)$  as obtained from CMS and LHCb [48–50] indicate  $\text{Br}(B_s \rightarrow \mu^+ \mu^-) = [2.9 \pm 0.7] \times 10^{-9}$ , which at  $3\sigma$  level leads to

$$0.8 \times 10^{-9} \leq \text{Br}(B_s \rightarrow \mu^+ \mu^-) \leq 5 \times 10^{-9}. \quad (3.4)$$

We compute the above B-Physics results using **SuperIso** [51] while using **SuSpect**[52] as the spectrum generator. In the following subsection we go beyond the generic region of pMSSM parameter space of Refs.[28–30], and explore the role of large  $|\mu|$  and large  $|A_t|$  in the context of the discussion made in Sec.2.

---

<sup>4</sup>We also remind the reader the additional issue of uncertainty of about 2.8 GeV in  $m_t^{\text{pole}}$  as argued in Ref.[45, 46].

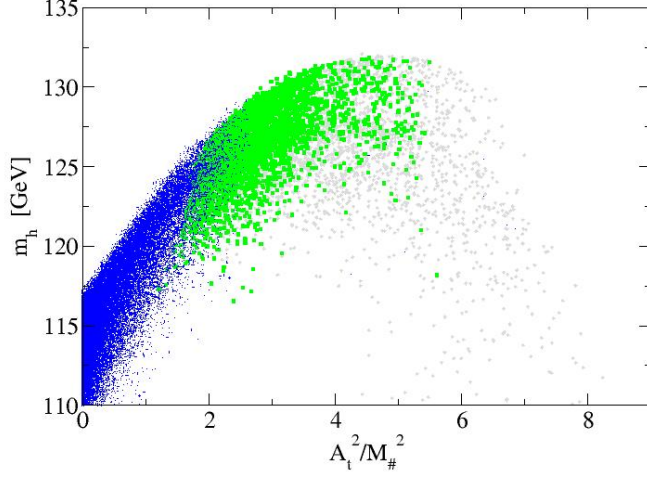


**Figure 1.** The variation of  $m_h$  against  $A_t^2/M_{\#}^2$  for the scanning ranges of Eq.3.1. Blue, green, grey dots correspond to stable, long-lived and short-lived vacua respectively. The first two type will comprise “safe” vacuum.

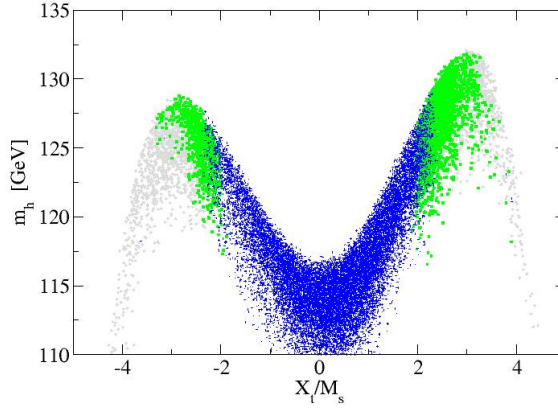


**Figure 2.** The variation of  $m_h$  vs  $X_t/M_s$  for the scanning ranges of 3.1. Blue, green and grey dots corresponds to stable, long-lived and short-lived vacua respectively.

### 3.2 Stability of vacuum for a fixed $\tan\beta$ and a large $|\mu|$

In order to analyze with large values of  $|\mu|$  we must remember that radiative corrections to Higgs boson mass from sbottom and to a lesser degree from stau sectors may hardly be ignored. This is because of a quartic dependence on  $|\mu|\tan\beta$  [53, 54] which is albeit suppressed by a quartic dependence of scalar masses, in addition to the effect of smallness of  $m_b$  or  $m_\tau$  compared to  $m_t$ .

Similar to Eq.2.3 the corrections from sbottom sector read[53, 54],

$$\Delta m_{h,bottom}^2 = \frac{3g_2^2 \bar{m}_b^4}{8\pi^2 M_W^2} \left[ \ln \left( \frac{m_{\tilde{b}_1} m_{\tilde{b}_2}}{\bar{m}_b^2} \right) + \frac{X_b^2}{m_{\tilde{b}_1} m_{\tilde{b}_2}} \left( 1 - \frac{X_b^2}{12m_{\tilde{b}_1} m_{\tilde{b}_2}} \right) \right], \quad (3.5)$$

where  $X_b = A_b - \mu \tan \beta$ <sup>5</sup>. Henceforth we allow sbottom fields in addition to stop fields to acquire non-zero *vevs* besides the Higgs fields within **Vevacious**. We fix  $\mu$  at 9 TeV,  $M_A$  at 1 TeV and  $\tan \beta = 20$ . Our range of scanning as given below involves parameters related to the stop and the sbottom sectors.

$$\begin{aligned} 500 &\leq m_{\tilde{Q}_3} \leq 3000 \text{ GeV}, \\ 500 &\leq m_{\tilde{U}_3} \leq 3000 \text{ GeV}, \\ 500 &\leq m_{\tilde{D}_3} \leq 3000 \text{ GeV}, \\ -10 &\leq A_t \leq 10 \text{ TeV}, \\ -10 &\leq A_b \leq 10 \text{ TeV}. \end{aligned} \quad (3.6)$$

We keep all other scalar mass parameters fixed at 1 TeV. We focus on a pocket of pMSSM parameter space as a representative zone that satisfy the cold dark matter constraints from WMAP[55]/PLANCK[56]. This corresponds to the following gaugino mass parameters

$$M_1 = 500 \text{ GeV}, M_2 = 525 \text{ GeV}, M_3 = 1400 \text{ GeV}. \quad (3.7)$$

Our choice of  $M_3$  is consistent with the recent limits on  $m_{\tilde{g}}$ [57]. The generic overabundance of a bino-like lightest neutralino dark matter which is the lightest supersymmetric particle (LSP) is brought under control via appropriate bino-wino ( $\tilde{B} - \tilde{W}$ ) coannihilation[58, 59]. This choice also satisfies the LUX[60] limit for the spin-independent direct detection cross section  $\sigma_{\chi p}^{SI}$ . Both the relic density and  $\sigma_{\chi p}^{SI}$  are computed using **micrOMEGAs**[61].

---

<sup>5</sup>A similar result for the stau contribution would involve  $X_\tau = A_\tau - \mu \tan \beta$ .

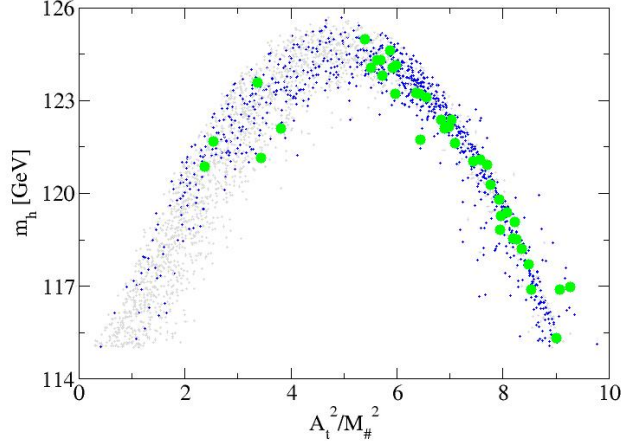


**Figure 3.** Plot of  $m_h$  vs  $A_t^2/M_{\#}^2$  corresponding to the scan of Eq.3.6 for  $\mu = 9$  TeV. Green, blue and grey dots correspond to long-lived, stable and short-lived SML vacuum states respectively. The points are spread throughout the plane without much clustering effect unlike Fig.1. Lack of clustering and appearance of long-lived states in the right half of the figure clearly shows the absence of validity of Eqs.2.4 and 2.6 when  $\mu$  is considered appreciably large.

In Fig. 3 we show the variation of  $m_h$  against  $A_t^2/M_{\#}^2$  corresponding to the scan of Eq.3.6 for  $\mu = 9$  TeV. Green, blue and grey dots that satisfy all the experimental limits mentioned above correspond to long-lived, stable and short-lived SML like vacuum respectively. Unlike Fig.1, the points are spread throughout the plane without much clustering effect. Lack of clustering and appearance of long-lived vacuum in the right half of the figure clearly shows the absence of validity of Eqs.2.4 and 2.6 when  $\mu$  is considered appreciably large.

### 3.3 Scan over wide range of $\mu$ and $A_t$ for $\tan\beta = 20$

In order to probe the impact of  $\mu$  and  $A_t$  on the stability of vacuum we scan over the same parameters in a wide range for a given set of pMSSM input values. Considering  $\tan\beta = 20$ , we fix  $m_{\tilde{Q}_3}, m_{\tilde{U}_3}, m_{\tilde{D}_3}$  at 2 TeV. All other sfermion masses are fixed at 1 TeV and  $M_A$  is taken to be 1 TeV. While allowing  $\tilde{t}_L, \tilde{t}_R, \tilde{b}_L$  and  $\tilde{b}_R$  to acquire non-zero  $v_{evs}$  along with the Higgs fields we choose the following range for  $\mu$  and  $A_t$ .

$$\begin{aligned} -10 \text{ TeV} &\leq A_t \leq 10 \text{ TeV}, \\ -11 \text{ TeV} &\leq \mu \leq 11 \text{ TeV}. \end{aligned} \quad (3.8)$$

We should keep in mind the importance of non-vanishing  $A_b$  in context of vacuum stability in CCB scenario, particularly for large  $\mu$  zones away from the generic region. However, non-vanishing  $A_b$  would hardly have an effect on  $m_h$ . Hence we use the following range for  $A_b$  namely,  $-6$  TeV to  $6$  TeV and consider vanishing trilinear couplings except  $A_t$ . Similar to Sec.3.2 we choose the

same gaugino mass parameters, whereas we impose B-Physics constraints of Eqs. 3.3 and 3.4 on the resulting spectrum as before.

In Fig. 4 we show the distribution corresponding to safe and dangerous SML vacua in the  $\mu - A_t$  plane. The central blue zone denotes the stable vacuum and the surrounding green strip represents the long-lived SML vacuum states. It is evident that the above zone that also includes small values of  $\mu$ , referred in this analysis as generic zone, is symmetric over both  $\mu$  and  $A_t$ . This implies that in the central zone, the stability of SML vacuum against decay to deeper CCB states is largely independent of the sign of  $\mu$  and  $A_t$ . For larger  $|\mu|$  within the central blue region, we see that safe vacua occur for smaller value of  $|A_t|$  and vice-versa.

Surrounding the central blue zone and the associated green peripheral region, one finds large grey regions designating short-lived vacuum states in which there also exist pockets of stable and long-lived zones in all the four quadrants. We further see the existence of stable/long-lived states for very large positive values of  $\mu$  and  $A_t$ , which would however be excluded by the traditional analytic constraints. Thus in Fig. 4 where we have used constraints from B-physics but not the Higgs mass bound, we find that SML minima is extended to island areas with appreciably large positive values of both  $\mu$  and  $A_t$ . We will later show that the island region of long-lived states with large  $\mu$  and  $A_t$  may also satisfy the Higgs mass limits. We particularly focus on the long-lived states<sup>6</sup> for the island region in the first quadrant and ignore any conclusion on the stable states in the same zone. This is connected to the fact that declaring a parameter point to be stable in the island region characterized by large  $\mu$  may be quite non-trivial due to various computational issues<sup>7</sup>.

### 3.3.1 Maximized $m_h$ zones in relation to long-lived states: Regions I and II

In Fig. 5 we show the effect of the same scanning (Eq.3.8) on Higgs boson mass  $m_h$ . In Fig. 5(a) we show the blue, green and grey regions in  $m_h$ - $\mu$  plane. One finds symmetric distribution about the  $\mu$ -axis within the large triangular green area. Short-lived vacuum states denoted by grey dots occupy the region outside the green strip of long-lived states.

We now identify the parameter region in  $\mu - A_t$  plane in relation to where  $m_h$  maximizes i.e. becomes close to the upper edge of Eq.3.2 as far as possible. We further check whether the maximized zones satisfy the traditional CCB constraints of Eqs.2.4, 2.6 or whether they fall into the category of long-lived vacuum states. Hence, for the above purpose, staying within the valid band of  $m_h$  (Eq.3.2) we would particularly like to focus on two regions in Fig. 5(a). Region-I (long-lived) is identified with  $|\mu| \simeq 1$  TeV and  $m_h \sim 128$  GeV (we would call this as small  $\mu$  zone), whereas Region-II (long-lived) occurs with  $7 \lesssim \mu \lesssim 9$  TeV and  $123 \lesssim m_h \lesssim 125$  GeV (we would refer it as the large  $\mu$  zone). For Fig. 5(b) the same regions of Fig.5(a) namely, Region-I maps to  $A_t \sim \pm 4$  TeV, whereas Region-II is characterized by  $3 \lesssim A_t \lesssim 5$  TeV. Both Regions I and II are generally ruled out by at least one of the traditional CCB constraints of Eqs. 2.4 and 2.6 but they correspond to long-lived vacuum

<sup>6</sup>We have discarded the parameter points that typically give warning messages related to appearance of saddle points.

<sup>7</sup>Private communication with the authors of **Vevacious**.

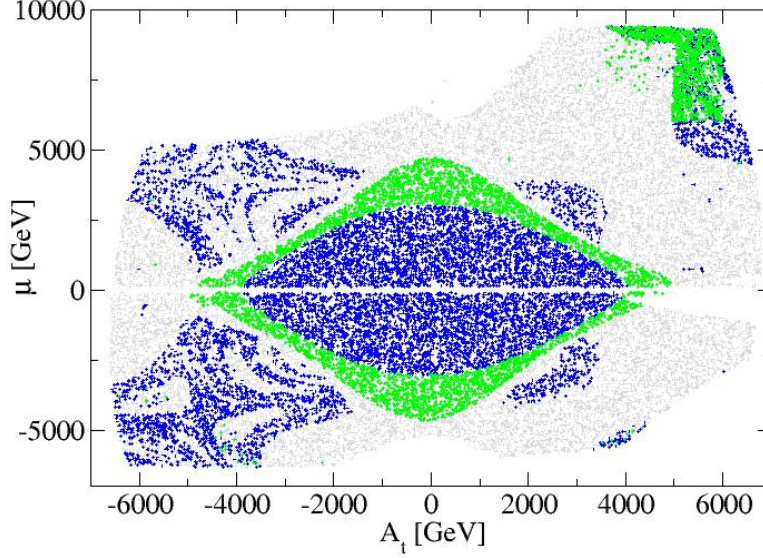


**Figure 4.** Plot of  $\mu$  vs  $A_t$  for  $\tan\beta = 20$  with fixed pMSSM parameters described in the beginning of Sec.3.3. Green, blue, grey dots corresponds to long-lived, stable and short-lived SML vacuum states. The central zone of stable states and the surrounding strip of long-lived states include the generic region of pMSSM parameter space, that is characterized by comparatively lower value of  $\mu$ . Interestingly there exist pockets of safe vacuum states in the zone much away from the central region, where traditional CCB constraints of Eqs.2.4 or 2.6 are violated.

states. We further point out that although  $m_h$  maximizes in Region-II for a given value of  $\mu$ , the corresponding value of  $X_t$  appreciably differs from  $\sqrt{6}M_S$  associated with an  $m_h^{max}$  scenario[6]. This is indeed related to the discussion made regarding the radiative corrections to  $m_h$  in Sec-2 specific to large values of  $\mu$ . Quite expectedly one finds that the relation  $X_t \simeq \sqrt{6}M_S$  holds good for low  $|\mu|$  belonging to Region-I. In Fig. 5(b) similar to Fig. 2,  $m_h$  maximizes for large positive values of  $A_t$ . Located symmetrically opposite to positive values of  $A_t$ , there is also a maximum of Higgs mass in the negative  $A_t$  region. This corresponds to a comparatively smaller value of  $m_h$  in a long-lived vacuum scenario.

Fig.6 is similar to Fig. 4 but here we impose the limits on  $m_h$  from Eq.3.2 and consider only the safe vacua in the  $\mu - A_t$  plane. As expected, there is no valid region below  $|A_t| = 2$  TeV. There exists a significant area with large  $\mu$  and large  $A_t$  with stable (blue dots) and long-lived states (green dots) that satisfy the Higgs mass data. As mentioned before, most of the above regions on the other hand, would be excluded by the traditionally used CCB constraints of Eq. 2.4 or 2.6. Thus the pMSSM parameter space can safely be extended to the above zone of large  $|\mu|$  and large  $|A_t|$ . Since the latter zone corresponds to Region-II of Fig.5(a) we infer that a maximized  $m_h$  occurring in a



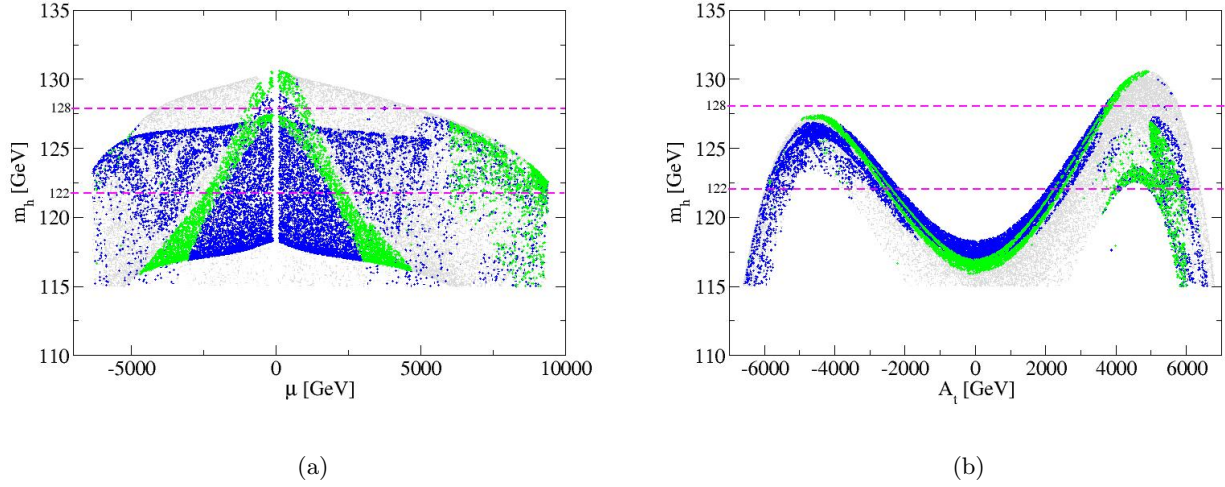


**Figure 5.** *Fig.5(a) shows the result of scanning described at the beginning of over  $A_t$  in the plane of  $m_h - \mu$  for  $\tan \beta = 20$ . The color codes for different vacuum stability conditions are same as that of Fig: 4. This confirms the existence of stable and long-lived vacua (satisfying Higgs mass limits) in the region characterized by large values of  $\mu$ . Fig.5(b) shows the result of scanning over  $\mu$  in the plane of  $m_h - A_t$ . It turns out that there can be stable and long-lived states for large  $|\mu|$  and/or large  $|A_t|$  that would not satisfy the traditional CCB constraints of Eqs.2.4 or 2.6. See text for Region-I and Region-II in relation to this figure.*

region away from  $X_t \simeq \sqrt{6}M_S$  would certainly require relatively smaller top-squark masses for a given amount of radiative corrections to the Higgs mass(see Eq.2.3). We note that the requirement to satisfy the limits of  $m_h$  eliminates i) small to moderate  $|A_t|$  zones and ii) regions with small  $|\mu|$  and very large  $A_t$ .

### 3.3.2 Compatibility with dark matter related constraints

We now briefly discuss the compatibility of our parameter space with dark matter related data such as the relic density limits from WMAP[55]/PLANCK[56] and spin-independent direct detection  $\tilde{\chi}_1^0 - p$  cross-section measurement from LUX [60].

Figs.7 shows the scatter plot of  $\sigma_{\chi p}^{SI}$  vs  $m_{\tilde{\chi}_1^0}$  with usual color codes. Only a few points within the thin vertical lines near  $m_{\tilde{\chi}_1^0} \simeq 500$  GeV satisfy the relic density ( $\Omega_{\tilde{\chi}_1^0} h^2$ ) limits, shown in orange. The imposed limits shown below at the level of  $5\sigma$  of PLANCK [56] data accommodates well the range given by WMAP [55].

$$0.092 \leq \Omega_{\tilde{\chi}_1^0} h^2 \leq 0.138. \quad (3.9)$$

We note that scattered points are clustered around two thin lines. It turns out that consideration of both signs of  $\mu$  and  $A_t$  leads to the appearance of two closely spaced lines. This is concerned with the slight dependence of the the radiative corrections to the mass of LSP[62–64] on the signs of  $\mu$ ,  $A_t$  and the dependence of  $\sigma_{\chi p}^{SI}$  on the sign of  $\mu$ [65].



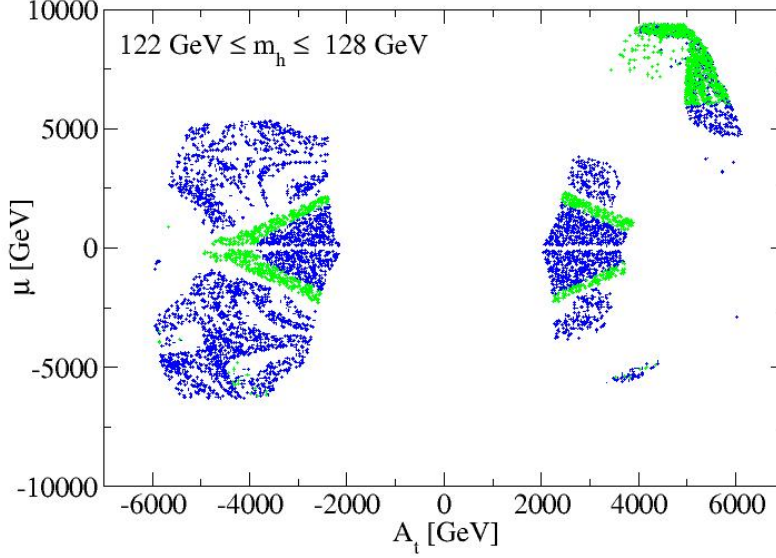


**Figure 6.** Plot of  $\mu$  vs  $A_t$  for  $\tan\beta = 20$  after imposing limits on  $m_h$  from Eq.3.2. Blue and green dots represent stable and long-lived vacuum states respectively. It turns out there is a significant region of long-lived states much away from the central region, where the traditional CCB constraints of Eqs.2.4 or 2.6 are violated. The requirement to satisfy the limits of  $m_h$  eliminates the small to moderate  $|A_t|$  zones and the regions with small  $|\mu|$  and very large  $A_t$  due to radiative corrections to the Higgs boson mass.

We emphasize here that giving *vevs* to several scalar fields within **Vevacious** demands a large increase in computational time of the analysis. Hence, we could not afford to scan the gaugino mass parameters  $M_1$  and  $M_2$  that have immediate effects on  $m_{\tilde{\chi}_1^0}$ . Thus, we only probe the acceptability of the chosen point in the  $M_1 - M_2$  plane while we scan the specific pMSSM parameters relevant to CCB constraints. Our analysis involves a wide variation over the value of  $\mu$ . Hence, there are only a few points where one has  $|\mu| < M_1$  for the chosen value  $M_1 = 500$  GeV. These are the parameter points where the relic density is very small because of a strong presence of Higgsino within the LSP. At the same time, in the region of  $\mu$  not far from  $M_1$  or  $M_2$ , there can be a large bino-higgsino or even bino-wino-higgsino mixing which leads to a larger value of  $\sigma_{\chi p}^{SI}$ [66]. This is confirmed in Fig. 7 that shows larger  $\sigma_{\chi p}^{SI}$  for  $m_{\tilde{\chi}_1^0}$  below 480 TeV or so, mostly exceeding the LUX data [60]. On the other hand, for larger values of  $|\mu|$  when the LSP becomes almost a bino, we expect  $\sigma_{\chi p}^{SI}$  to be small, a fact confirmed by the figure. A part of the above region characterized by small  $\sigma_{\chi p}^{SI}$  provides correct relic density via bino-wino coannihilation[66, 67]. We comment that our chosen values of  $M_1$  and  $M_2$  that is consistent with WMAP/PLANCK data would only be probed in future experiments like XENON1T[68]. We like to point out that our analysis could be carried out for other appropriate gaugino masses that would satisfy the relic density and would result into

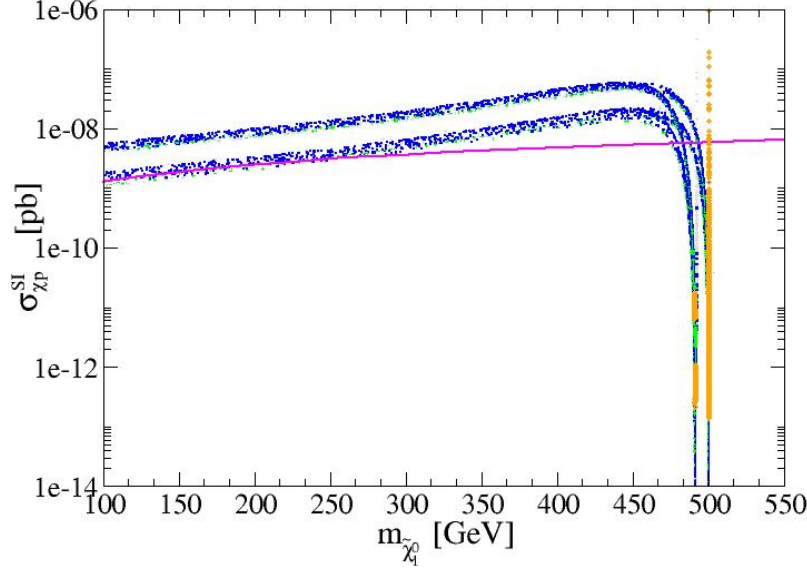


**Figure 7.** Plot of  $\sigma_{\chi p}^{SI}$  vs  $m_{\tilde{\chi}_1^0}$  for the scan of Sec.3.3. The region above the pink line is excluded by the LUX limits on  $\sigma_{\chi p}^{SI}$  [60]. For  $|\mu| < M_1$ , there is a significant Higgsino content in  $\tilde{\chi}_1^0$ . Consequently  $\sigma_{\chi p}^{SI}$  is large and  $\Omega_{\tilde{\chi}_1^0} h^2$  is low. The presence of two branches is attributed to slight dependence of  $\sigma_{\chi p}^{SI}$  on the sign of  $\mu$  that we have varied during the analysis. The orange colored region represents the zone with proper relic abundance as mentioned in Eq. 3.9. In these regions with adequate dark matter abundance and allowed  $\sigma_{\chi p}^{SI}$ ,  $\tilde{\chi}_1^0$  is  $\tilde{B}$  dominated. Adequate relic abundance is obtained via  $\tilde{B} - \tilde{W}$  coannihilation. Most of the points characterized by small  $\sigma_{\chi p}^{SI}$  cluster around two values of  $m_{\tilde{\chi}_1^0}$  separated by a small amount. This is due to the dependence of the radiative corrections to  $m_{\tilde{\chi}_1^0}$  on the sign of  $\mu$  as well as on  $A_t$  (via stop mass).

$\sigma_{\chi p}^{SI}$  in the vicinity of the sensitivity region of LUX or future XENON1T experiments.

### 3.4 Scan over wide range of $\mu$ and $A_t$ for $\tan\beta = 40$

The role of  $\tan\beta$  in studies related to vacuum stability is important via its effect on the scalar potential as well as due to its influence on the radiative corrections to the mass of the Higgs boson, specially for large  $\mu$  scenarios. In the context of Eq.3.5 the sbottom and even the stau loop contributions become important for large values of  $\mu \tan\beta$  and it is revealed that these have negative contributions to  $m_h$  that can potentially reduce  $m_h$  below the lower limit of Eq.3.2. Thus in this part of our work with  $\tan\beta = 40$  we choose a larger value (3 TeV) for the third generation of squark mass parameter in order to respect the Higgs mass limits, while keeping the same values of other pMSSM parameters of Sec.3.3. The combined sbottom and stau loop contributions typically amounts to 10-15 percent within the range of Higgs boson mass of Eq.3.2. Along with the Higgs fields, we again allow  $\tilde{t}_L, \tilde{t}_R, \tilde{b}_L$  and  $\tilde{b}_R$  to acquire non-zero *vevs* and choose the following ranges

for  $\mu$ ,  $A_t$  and  $A_b$ .

$$\begin{aligned}
-10 \text{ TeV} &\leq A_t \leq 10 \text{ TeV}, \\
-6 \text{ TeV} &\leq A_b \leq 6 \text{ TeV}, \\
-7 \text{ TeV} &\leq \mu \leq 7 \text{ TeV} .
\end{aligned} \tag{3.10}$$

As before we consider vanishing trilinear couplings except  $A_t$  and  $A_b$ . Compared to the case of  $\tan\beta = 20$ , here the range of  $\mu$  giving valid parameter point becomes smaller because of the Higgs mass limits as mentioned above. Similar to Sec.3.2 we impose B-Physics constraints of Eqs. 3.3, 3.4 on the resulting spectrum.

Fig.8 shows the result of parameter scanning in the plane of  $\mu - A_t$  where we have not used the constraints of Higgs mass limits. A significant region of parameter space for large and positive  $A_t$ , particularly for  $\mu < 0$  is eliminated via  $\text{Br}(B \rightarrow X_s \gamma)$  limits. This typically happens due to cancellation between the chargino and the combined contributions of  $t - W$  loop from SM along with charged Higgs loops. This may reduce the above branching ratio to values smaller than the lower limit of Eq.3.3. This is consistent with the expected result of  $\text{Br}(B \rightarrow X_s \gamma)$  for  $\mu A_t < 0$ [54, 69, 70]. Similarly a large amount of parameter zone of the same quadrant is eliminated via  $\text{Br}(B_s \rightarrow \mu^+ \mu^-)$  which becomes sensitive for large  $\tan\beta$ [71], in spite of the fact that the pseudoscalar Higgs mass is quite large. We note that the above agrees with the analysis of Ref.[69] where  $\text{Br}(B_s \rightarrow \mu^+ \mu^-)$  for a large  $\tan\beta$  is seen to be enhanced for  $\mu A_t < 0$ . Interestingly, in contrast to Fig.4 here the safe vacua are almost exclusively long-lived in the large  $\mu$  and large  $A_t$  region.

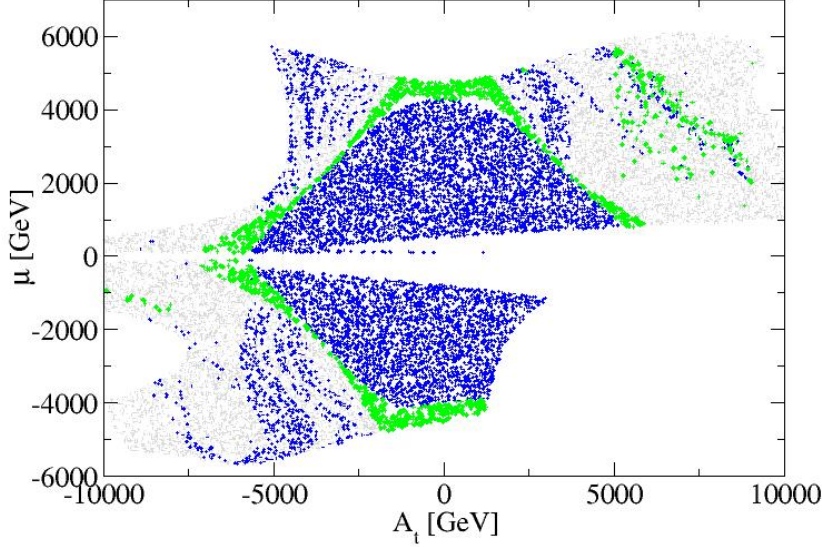


**Figure 8.** Plot of  $\mu$  vs  $A_t$  for  $\tan\beta = 40$  and other fixed  $p\text{MSSM}$  parameters as described in the beginning of Sec.3.4. The color codes for different vacuum stability conditions are same as that of Fig. 4. The central zone of stable states and the surrounding strip of long-lived states include the generic region of  $p\text{MSSM}$  parameter space, that is characterized by relatively smaller value of  $|\mu|$ . There exist pockets of long-lived states quite distant from stable states in the zone much away from the central region. A significant region of parameter space for large and positive values of  $A_t$ , particularly for  $\mu < 0$  is eliminated via  $\text{Br}(B \rightarrow X_s \gamma)$  and  $\text{Br}(B_s \rightarrow \mu^+ \mu^-)$  limits (see text).

A similar result when projected into  $m_h - \mu$  plane is shown in Fig.9(a). As in Fig.5(a) we obtain two distinct regions namely Region-I and Region-II of long-lived vacua corresponding to small and large  $\mu$  respectively for maximized  $m_h$  cases. Region-I (long-lived) is identified with  $\mu \simeq 1$  TeV and  $m_h \simeq 127$  GeV (small  $\mu$  zone) whereas Region-II (long-lived) occurs with  $4 \text{ TeV} < \mu < 5.5 \text{ TeV}$  and  $122 \text{ GeV} \lesssim m_h \lesssim 128 \text{ GeV}$  (large  $\mu$  zone). Going from  $\tan\beta = 20$  to  $\tan\beta = 40$  we see that  $|\mu|$  cannot assume very large values because this would lead to a rapid decrease of  $m_h$  when  $\mu$  is increased, via radiative corrections from the sbottom and stau loops (Eq.3.5). With the same parameter scan, Fig.9(b) is similar to Fig.5(b) except that it refers to  $\tan\beta = 40$  along with a heavier third generation of squarks. Unlike Fig.5(b) here the EWSB vacuum is mostly long-lived for large values of  $A_t$  which also spans a larger range.

In Fig.10 we show the distribution of parameter points for stable and long-lived vacua in  $\mu - A_t$  plane where  $m_h$  lies in the range of Eq.3.2. The areas corresponding to stable states in different quadrants are appreciably shrunk for this case of a large  $\tan\beta$ . On the other hand, the EWSB SML vacua in large  $\mu$  and large  $A_t$  region which are also distinctly isolated (green) in the figure

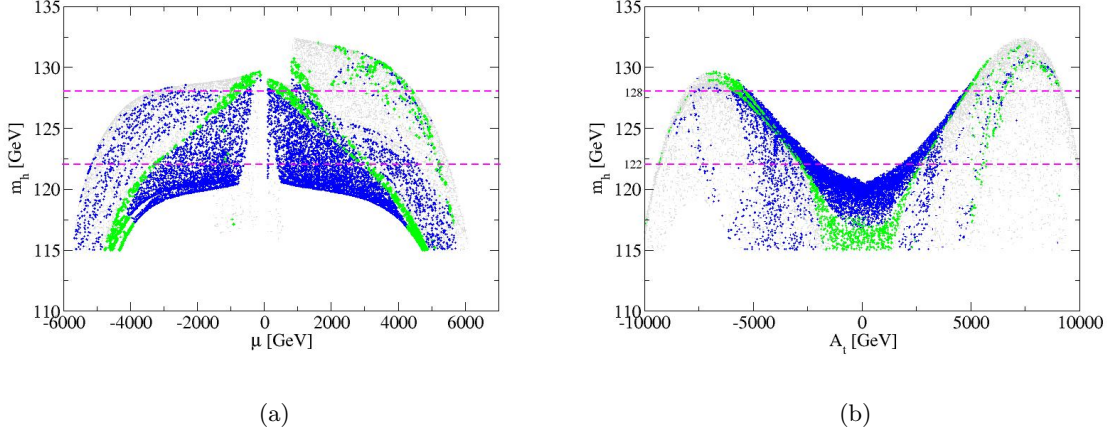


**Figure 9.** *Fig.9(a) shows the result of scanning over  $A_t$  for  $\tan\beta = 40$  in the plane of  $m_h - \mu$  for the fixed  $p$ MSSM parameters as described in the beginning of Sec.3.4. The color codes for different vacuum stability conditions are same as that of Fig: 4. As in Fig.5(a) we also identify two distinct regions namely Region-I and Region-II of long-lived vacua corresponding to small and large  $\mu$  respectively for maximized  $m_h$  (see text). Fig.9(b) shows the result in the plane of  $m_h - A_t$ . Here  $A_t$  spans a larger zone compared to the case of  $\tan\beta = 20$  of Fig.5(b) (see text).*

are mostly long-lived unlike the case of  $\tan\beta = 20$ . For very large values of  $|\mu|$ , long-lived states are associated with large values of  $|A_t|$ . We note that the requirement to satisfy the limits of  $m_h$  eliminates the small to moderate  $|A_t|$  zones and the regions with small  $|\mu|$  and very large  $A_t$  due to radiative corrections. The latter combination enhances  $m_h$  to cross the upper bound of Eq.3.2.

We now briefly discuss the compatibility of our analysis of  $\tan\beta = 40$  with dark matter related data for the relic density limits from WMAP[55]/PLANCK[56] and spin-independent direct detection  $\tilde{\chi}_1^0 - p$  cross-section measurement from LUX [60]. Fig.11 shows the variation of  $\sigma_{\chi p}^{SI}$  with  $m_{\tilde{\chi}_1^0}$ . The region above the pink line is excluded by LUX results. The regions with adequate  $\Omega_{\tilde{\chi}_1^0} h^2$  as constrained by Eq.3.9 is shown in orange dots. The other features of Fig.11 are similar to what is described for Fig.7.

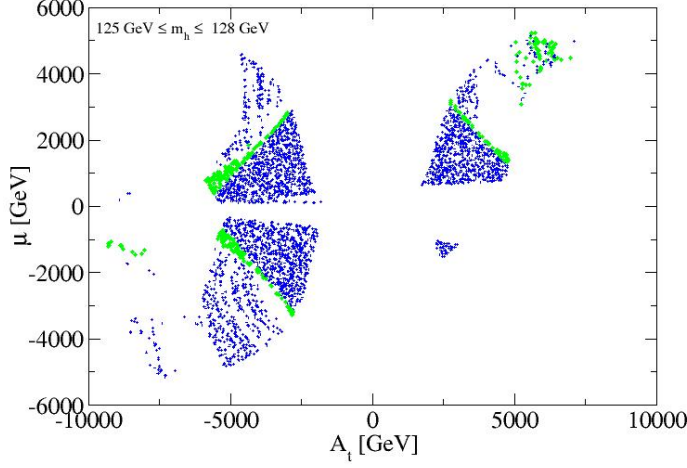


**Figure 10.** Plot of  $\mu$  vs  $A_t$  for  $\tan \beta = 40$  after imposing limits on  $m_h$  from Eq. 3.2. The areas corresponding to stable states in different quadrants are appreciably shrunk for this case of a large  $\tan \beta$ . The EWSB SML vacuum states in large  $\mu$  and large  $A_t$  region which are also distinctly identified are mostly long-lived unlike the case of  $\tan \beta = 20$ . For very large values of  $|\mu|$ , long-lived states are associated with large values of  $|A_t|$ . The requirement to satisfy the limits of  $m_h$  eliminates small to moderate  $|A_t|$  zones and the regions with small  $|\mu|$  and very large  $A_t$  due to radiative corrections in  $m_h$  (see text).

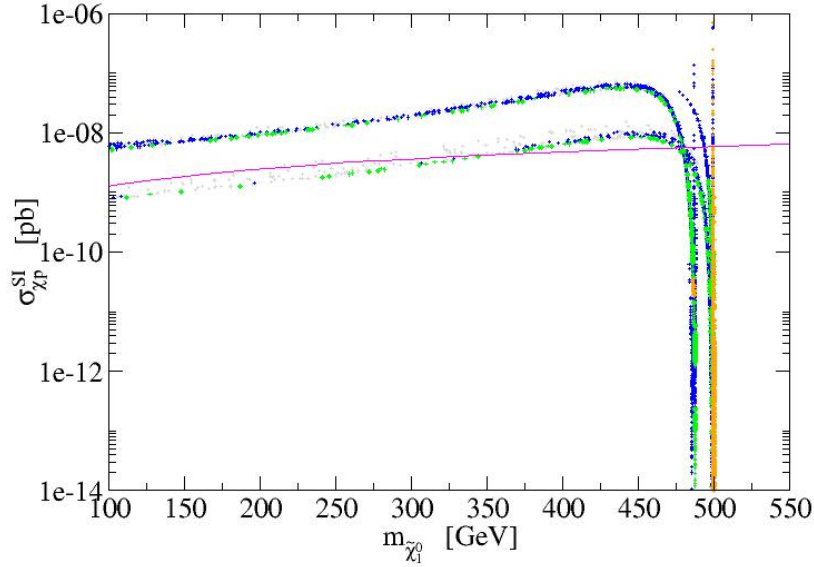


**Figure 11.** Plot of  $m_{\tilde{\chi}_1^0} - \sigma_{\chi p}^{SI}$  for  $\tan \beta = 40$  of the analysis of Sec. 3.4. See text and caption of Fig. 7 for further details.

### 3.5 Muon $g - 2$

Finding both large  $\mu$  and small  $|\mu|$  regions corresponding to Region-II and Region-I respectively as referred before, to be valid long-lived vacuum states we immediately like to relate this to the issue of satisfying the constraint from Muon Anomalous Magnetic Moment. At one-loop level, the supersymmetric contributions to  $a_\mu$  with  $a_\mu = \frac{1}{2}(g - 2)_\mu$  [72, 73] originate from chargino-sneutrino and neutralino-smuon loops. Large contributions may come from neutralino-smuon loops when  $\mu$  is large along with smaller slepton masses [74]. On the other hand, for small  $\mu$  zones smaller masses of charginos would increase the supersymmetric contributions  $a_\mu^{SUSY}$  to  $a_\mu$ . The experimental data ( $\equiv a_\mu^{exp}$ ) [75, 76] differs significantly from SM prediction ( $\equiv a_\mu^{SM}$ ) [77, 78] leading to the following result where errors are added in quadrature.

$$a_\mu^{SUSY} = \Delta a_\mu = a_\mu^{exp} - a_\mu^{SM} = (29.3 \pm 9.0) \times 10^{-10}. \quad (3.11)$$

At the level of  $2\sigma$  one has,

$$11.3 \times 10^{-10} < a_\mu^{SUSY} < 47.3 \times 10^{-10}. \quad (3.12)$$

Focusing on muon  $g - 2$  constraint for a  $2\sigma$  limit, we now present Table 1 for four benchmark points, two each for  $\tan\beta = 20$  and 40. These are associated with long-lived states corresponding to Region-I and Region-II as mentioned before. The point for  $\tan\beta = 20$  in Region-I corresponding to smaller  $\mu$  satisfies  $a_\mu^{SUSY}$  constraint of Eq. 3.12 principally because of smaller lighter chargino mass [74]. For the Region -I point corresponding to  $\tan\beta = 40$ , there is a natural enhancement of  $a_\mu^{SUSY}$  due to larger  $\tan\beta$ . As a result a larger lighter chargino mass could be accommodated. For the long-lived state associated with Region-II, where  $\mu$  is large, smaller values of slepton masses are required in order to satisfy Eq. 3.12 because  $\mu$  is large. This is connected with the larger contribution from the neutralino-smuon part of the diagrams for  $a_\mu^{SUSY}$  [74]. The contributions from the above type of diagram is more dominant for  $\tan\beta = 20$  where  $\mu$  is much larger than the case of  $\tan\beta = 40$ . However, for the two points belonging to Region-II an increase in  $a_\mu^{SUSY}$  due to an increase in  $\tan\beta$  is counterbalanced by a decrease in  $\mu$ , since  $\mu$  spans a smaller zone for  $\tan\beta = 40$ .

Finally, we would like to comment that for the benchmark point of Region-II corresponding to  $\tan\beta = 20$ , the lighter top-squark mass in particular is adequately light that in turn arises out of a sufficiently large  $\mu$ . The largeness of  $\mu$  indeed causes negative contributions to the radiative corrections to Higgs boson mass via sbottom and stau loops as discussed before. This effectively reduces  $m_h$  which on the other hand allows to accommodate a larger  $A_t$ . The latter in turn gives rise to a lighter  $\tilde{t}_1$  via left-right mixing. Similar effect for  $\tan\beta = 40$  also holds good but is limited via smaller value of  $\mu$  that is allowed via vacuum stability requirement for long-lived states with proper Higgs mass.



**Table 1.** *Benchmark points for long-lived vacuum states*

Parameters	∈ Region I	∈ Region II	∈ Region I	∈ Region II
$m_{1,2,3}$	160, 179, 1400	500, 525, 1400	490, 550, 1400	500, 525, 1400
$m_{\tilde{Q}_3}/m_{\tilde{U}_3}/m_{\tilde{D}_3}$	<b>2000</b>	<b>2000</b>	<b>3000</b>	<b>3000</b>
$m_{\tilde{Q}_2}/m_{\tilde{U}_2}/m_{\tilde{D}_2}$	1000	1000	1000	1000
$m_{\tilde{Q}_1}/m_{\tilde{U}_1}/m_{\tilde{D}_1}$	1000	1000	1000	1000
$m_{\tilde{L}_3}/m_{\tilde{E}_3}$	1000	1000	1000	1000
$m_{\tilde{L}_2}/m_{\tilde{E}_2}$	430	600	510	572
$m_{\tilde{L}_1}/m_{\tilde{E}_1}$	430	600	510	572
$A_t, A_b, A_\tau$	3500, 0, 0	5188.5, -2640.2, 0	4691.2, 0, 0	6273.4, -3040.7, 0
$\tan \beta$	<b>20</b>	<b>20</b>	<b>40</b>	<b>40</b>
$\mu$	1000	8831.0	1500.0	4940.2
$m_A$	1000	1000	1000	1000
$m_{\tilde{g}}$	1486.9	1486.7	1531.6	1531.6
$m_{\tilde{u}_L}$	1083.5	1083.2	1179.8	1107.9
$m_{\tilde{t}_1}, m_{\tilde{t}_2}$	1880.0, 2113.5	922.7, 1683.7	2870.1, 3088.2	2771.3, 3064.7
$m_{\tilde{b}_1}, m_{\tilde{b}_2}$	2035.2, 2054.8	1986.6, 2101.4	3023.6, 3060.8	2995.9, 3087.9
$m_{\tilde{e}_L}, m_{\tilde{\nu}_e}$	432.4, 425.3	601.8, 596.8	512.1, 506.1	573.4, 568.3
$m_{\tilde{\tau}_1}, m_{\tilde{\nu}_\tau}$	984.0, 998.0	838.8, 998.0	946.3, 998.0	810.8, 998.0
$m_{\tilde{\chi}_1^\pm}, m_{\tilde{\chi}_2^\pm}$	177.2, 1006.4	524.9, 8831.7	548.1, 1505.4	524.8, 4941.5
$m_{\tilde{\chi}_1^0}, m_{\tilde{\chi}_2^0}$	159.4, 177.3	500.0, 524.9	489.4, 548.1	500.0, 524.8
$m_{\tilde{\chi}_3^0}, m_{\tilde{\chi}_4^0}$	1003.1, 1005.4	8313.4, 8313.5	1502.5, 1505.1	4940.9, 4941.2
$m_{H^\pm}$	1003.5	1001.2	1003.4	1002.7
$m_H, m_h$	1000.0, 126.8	988.8, 122.1	1000.0, 127.5	999.5, 124.9
$\text{Br}(B \rightarrow X_s \gamma)$	$3.67 \times 10^{-4}$	$2.85 \times 10^{-4}$	$3.75 \times 10^{-4}$	$3.25 \times 10^{-4}$
$\text{Br}(B_s \rightarrow \mu^+ \mu^-)$	$3.17 \times 10^{-9}$	$3.23 \times 10^{-9}$	$1.85 \times 10^{-9}$	$1.95 \times 10^{-9}$
$a_\mu$	$11.9 \times 10^{-10}$	$12.0 \times 10^{-10}$	$11.8 \times 10^{-10}$	$16.5 \times 10^{-10}$
$\Omega_{\tilde{\chi}_1^0} h^2$	0.128	0.118	0.113	0.107
$\sigma_{\tilde{\chi}_1^0 \text{p}}^{\text{SI}}$ in pb	$3.74 \times 10^{-11}$	$1.82 \times 10^{-13}$	$3.92 \times 10^{-11}$	$9.07 \times 10^{-13}$

## 4 Conclusion

It is exciting that the Higgs boson has been discovered in LHC with its mass around 125 GeV which is well within the MSSM predicted upper limit of 135 GeV or so. However, such a relatively heavy Higgs boson is not so friendly in terms of the hierarchy problem. It is thus important to explore the MSSM parameter space that may still be associated with a relatively lighter SUSY spectra. The observed value requires large radiative corrections to the Higgs boson mass that is driven by the third generation scalars with large Yukawa couplings, particularly the top squarks. It is possible to

limit the latter to become not so heavy by considering large mixing between the left and the right scalar components. Choosing a large value of trilinear coupling  $|A_t|$  may induce large radiative corrections but this could be limited by the appearance of the Charge and Color Breaking Minima. It may be seen that the role of the higgsino mixing parameter  $\mu$  may be important in addition to  $A_t$  while discussing CCB constraint. We discussed the negative corrections from sbottom and stau loop contributions to the Higgs mass for large values of  $\mu \tan \beta$ . An effectively reduced value of  $m_h$  as such allows a wider zone of  $A_t$ , which in turn may reduce the top squark masses in a significant zone of MSSM parameter space.

Traditionally, appearance of global CCB minima is avoided via use of analytic relations like Eqs. 2.4 or 2.6 of Sec.2 as explored in the work of Casas *et al*[7]. Ref.[14, 18] and recently Ref.[21] considered the existence of long-lived vacuum states for which the transition to the global CCB minima requires a time larger than the age of the Universe. The above references hence used relaxed constraints like Eqs.2.7,2.8. However, by searching appropriate minima numerically and computing the transition time, it was shown in Refs.[27–30] that the analytic relations are neither sufficient nor necessary. We confirm their conclusions in a broader setup of considering all possible signs of  $\mu$  and  $A_t$  along with a wider scanning range for the above parameters using **Vevacious**. As with the above references we find that the long-lived states exist even in the region where the traditional CCB constraints are satisfied. Moreover, long-lived states extend to the zone where the traditional analytical constraints on CCB are violated. This only shows the necessity of analyzing CCB effects via numerical means. Since the third generation of sfermions with larger Yukawa couplings have immediate effect on the tunneling time we consider non-vanishing *vevs* for both stop and sbottom fields.

We find that in the generic region of pMSSM where  $|A_t|$  and  $|\mu|$  are comparatively smaller, distinct regions of stable and long-lived states exist irrespective of the signs of the above two parameters. Beyond the above generic pMSSM regions of stable and long-lived states there exist zones of dangerous vacua. Interestingly, we find safe vacua in a broad region of pMSSM parameter space with large  $|\mu|$  and  $|A_t|$ . Furthermore, among the above safe vacua zones one finds long-lived states that fall in the interesting zone where Higgs mass radiative corrections maximize. We note that the safe vacua for a large value of  $\tan \beta$  in large  $\mu$  and large  $A_t$  regions are found to be predominantly long-lived in nature. Additionally, we impose the constraints from  $\text{Br}(B \rightarrow X_s \gamma)$  and  $\text{Br}(B_s \rightarrow \mu^+ \mu^-)$ . A large region of parameter space with  $\mu A_t < 0$  is disfavoured by the above constraints specially for large  $\tan \beta$ . The interesting zone of long-lived vacuum states that is associated with large radiative corrections to the Higgs boson mass satisfy all the above constraints. On the other hand, it is also possible to satisfy the constraints from dark matter experiments by appropriately choosing pockets of parameter space in the gaugino sector which is essentially disjoint of our study related to CCB vacua. For economy of computation time we choose a combination of closely spaced U(1) and SU(2) gaugino masses that satisfy the WMAP/PLANCK data via binowino coannihilations. The corresponding direct detection cross section  $\sigma_{\chi p}^{SI}$  also satisfies the LUX

data. Finally, for our analysis with large  $A_t$  we find two distinct zones of long-lived states for small and large values of  $\mu$ . We extend the analysis by considering the possibility to satisfy the limits from muon  $g - 2$  for the above scenarios. It is found that limits from muon  $g - 2$  are satisfied via two distinct classes of diagrams contributing to  $a_\mu^{SUSY}$  for the two cases namely small and large  $\mu$ .

## 5 Acknowledgment

A.D. would like to thank the Council of Scientific and Industrial Research, Government of India for support. U.C. would like to thank Dr. Debtosh Chowdhury for a brief and useful discussion. A.D. and U.C. would like to thank Dr. Ben O’Leary for detailed discussion about a few important technical issues regarding Vevacious.

## References

- [1] E. S. Abers and B. W. Lee, Phys. Rept. **9**, 1 (1973); A. Sirlin, Nucl. Phys. B **196**, 83 (1982); T. P. Cheng and L. F. Li, Oxford, Uk: Clarendon ( 1984) 536 P. ( Oxford Science Publications); A. Djouadi, Phys. Rept. **457**, 1 (2008) [hep-ph/0503172].
- [2] For reviews on supersymmetry, see, *e.g.*, H. P. Nilles, Phys. Rep. **110**, 1 ( 1984); J. D. Lykken, hep-th/9612114; J. Wess and J. Bagger, *Supersymmetry and Supergravity*, 2nd ed., (Princeton, 1991).
- [3] M. Drees, P. Roy and R. M. Godbole, *Theory and Phenomenology of Sparticles*, (World Scientific, Singapore, 2005).
- [4] H. Baer and X. Tata, *Weak scale supersymmetry: From superfields to scattering events*, Cambridge, UK: Univ. Pr. (2006) 537 p.
- [5] D. J. H. Chung, L. L. Everett, G. L. Kane, S. F. King, J. D. Lykken and L. T. Wang, Phys. Rept. **407**, 1 (2005); H. E. Haber and G. Kane, Phys. Rep. **117**, 75 ( 1985) ; S. P. Martin, arXiv:hep-ph/9709356.
- [6] A. Djouadi, Phys. Rept. **459**, 1 (2008) [hep-ph/0503173].
- [7] J. A. Casas, A. Lleyda and C. Munoz, Nucl. Phys. B **471**, 3 (1996) [hep-ph/9507294].
- [8] C. Le Mouel, Phys. Rev. D **64**, 075009 (2001) [hep-ph/0103341]; C. Le Mouel, Nucl. Phys. B **607**, 38 (2001) [hep-ph/0101351].
- [9] L. Alvarez-Gaume, J. Polchinski and M. B. Wise, Nucl. Phys. B **221**, 495 (1983).
- [10] J. F. Gunion, H. E. Haber and M. Sher, Nucl. Phys. B **306**, 1 (1988).
- [11] A. Strumia, Nucl. Phys. B **482**, 24 (1996) [hep-ph/9604417].
- [12] H. Baer, M. Brhlik and D. Castano, Phys. Rev. D **54**, 6944 (1996) [hep-ph/9607465].
- [13] S. A. Abel and C. A. Savoy, Phys. Lett. B **444**, 119 (1998) [hep-ph/9809498]; S. Abel and T. Falk, Phys. Lett. B **444**, 427 (1998) [hep-ph/9810297]; P. M. Ferreira, hep-ph/0406234; M. Brhlik, Nucl. Phys. Proc. Suppl. **101**, 395 (2001).  
For details of one-loop CCB effective potential, see P. M. Ferreira, Phys. Lett. B **509**, 120 (2001) [Erratum-ibid. B **518**, 333 (2001)] [hep-ph/0008115].

- [14] A. J. Bordner, hep-ph/9506409.
- [15] D. G. Cerdeno, E. Gabrielli, M. E. Gomez and C. Munoz, JHEP **0306**, 030 (2003) [hep-ph/0304115].
- [16] A. Riotto and E. Roulet, Phys. Lett. B **377**, 60 (1996) [hep-ph/9512401].
- [17] T. Falk, K. A. Olive, L. Roszkowski, A. Singh and M. Srednicki, Phys. Lett. B **396**, 50 (1997) [hep-ph/9611325].
- [18] A. Kusenko, P. Langacker and G. Segre, Phys. Rev. D **54**, 5824 (1996) [hep-ph/9602414].
- [19] A. Kusenko and P. Langacker, Phys. Lett. B **391**, 29 (1997) [hep-ph/9608340]; A. Kusenko, Nucl. Phys. Proc. Suppl. **52A**, 67 (1997) [hep-ph/9607287]; A. Kusenko, Phys. Lett. B **358**, 51 (1995) [hep-ph/9504418].
- [20] R. H. Brandenberger, Rev. Mod. Phys. **57**, 1 (1985).
- [21] T. Cohen and J. G. Wacker, JHEP **1309**, 061 (2013) [arXiv:1305.2914 [hep-ph]].
- [22] J. E. Camargo-Molina, B. O’Leary, W. Porod and F. Staub, Eur. Phys. J. C **73**, 2588 (2013) [arXiv:1307.1477 [hep-ph]]. We have used version 1.0.11.
- [23] C. L. Wainwright, Comput. Phys. Commun. **183**, 2006 (2012) [arXiv:1109.4189 [hep-ph]].
- [24] G. Aad *et al.* [ATLAS Collaboration], Phys. Lett. B **716**, 1 (2012) [arXiv:1207.7214 [hep-ex]]; S. Chatrchyan *et al.* [CMS Collaboration], Phys. Lett. B **716**, 30 (2012) [arXiv:1207.7235 [hep-ex]].
- [25] S. Chatrchyan *et al.* [CMS Collaboration], JHEP **1306**, 081 (2013) [arXiv:1303.4571 [hep-ex]].
- [26] A. Djouadi *et al.* [MSSM Working Group Collaboration], hep-ph/9901246.
- [27] J. E. Camargo-Molina, B. O’Leary, W. Porod and F. Staub, JHEP **1312**, 103 (2013) [arXiv:1309.7212 [hep-ph]].
- [28] D. Chowdhury, R. M. Godbole, K. A. Mohan and S. K. Vempati, JHEP **1402**, 110 (2014) [arXiv:1310.1932 [hep-ph]].
- [29] N. Blinov and D. E. Morrissey, arXiv:1309.7397 [hep-ph].
- [30] J. E. Camargo-Molina, B. Garbrecht, B. O’Leary, W. Porod and F. Staub, arXiv:1405.7376 [hep-ph].
- [31] S. R. Coleman, Phys. Rev. D **15**, 2929 (1977) [Erratum-ibid. D **16**, 1248 (1977)]; C. G. Callan, Jr. and S. R. Coleman, Phys. Rev. D **16**, 1762 (1977). Also see Ref. [18] and references 12, 15 therein.
- [32] G. Jungman, M. Kamionkowski and K. Griest, Phys. Rept. **267**, 195 (1996) [hep-ph/9506380]; G. Bertone, D. Hooper and J. Silk, Phys. Rept. **405**, 279 (2005) [hep-ph/0404175]; L. Bergstrom, Annalen Phys. **524**, 479 (2012) [arXiv:1205.4882 [astro-ph.HE]]; K. Garrett and G. Duda, Adv. Astron. **2011**, 968283 (2011) [arXiv:1006.2483 [hep-ph]].
- [33] D. M. Pierce, J. A. Bagger, K. T. Matchev and R. -j. Zhang, Nucl. Phys. B **491**, 3 (1997) [hep-ph/9606211].
- [34] H. Komatsu, Phys. Lett. B **215**, 323 (1988); A. Datta, A. Kundu and A. Samanta, Phys. Rev. D **63**, 015008 (2001) [hep-ph/0007148]; A. Datta and A. Samanta, J. Phys. G **29**, 2721 (2003) [hep-ph/0108056]; A. Datta and A. Samanta, Phys. Lett. B **526**, 111 (2002) [hep-ph/0111222]; A. Datta and A. Samanta, Phys. Lett. B **607**, 144 (2005) [hep-ph/0406129]; E. Gabrielli, K. Huitu and S. Roy, Phys. Rev. D **65**, 075005 (2002) [hep-ph/0108246].

- [35] U. Ellwanger and C. Hugonie, Phys. Lett. B **457**, 299 (1999) [hep-ph/9902401]; T. Kobayashi and T. Shimomura, Phys. Rev. D **82**, 035008 (2010) [arXiv:1006.0062 [hep-ph]].
- [36] J. Hisano and S. Sugiyama, Phys. Lett. B **696**, 92 (2011) [Erratum-ibid. B **719**, 472 (2013)] [arXiv:1011.0260 [hep-ph]]; M. Carena, S. Gori, I. Low, N. R. Shah and C. E. M. Wagner, JHEP **1302**, 114 (2013) [arXiv:1211.6136 [hep-ph]].
- [37] T. Kitahara and T. Yoshinaga, JHEP **1305**, 035 (2013) [arXiv:1303.0461 [hep-ph]].
- [38] N. Sakai, Zeit. Phys. C **11** (1981) 153; R. K. Kaul and P. Majumdar, Nucl. Phys. B **199** (1982) 36; R. Barbieri and G. F. Giudice, Nucl. Phys. B **306** (1988) 63.
- [39] R. Barbieri and G. F. Giudice, Nucl. Phys. B **306**, 63 (1988); K. L. Chan, U. Chattopadhyay and P. Nath, Phys. Rev. D **58**, 096004 (1998); [arXiv:hep-ph/9710473]; J. L. Feng, K. T. Matchev and T. Moroi, Phys. Rev. D **61**, 075005 (2000); Phys. Rev. Lett. **84**, 2322 (2000) [arXiv:hep-ph/9908309]; U. Chattopadhyay, A. Corsetti and P. Nath, Phys. Rev. D **68**, 035005 (2003) [arXiv:hep-ph/0303201]; S. Akula, M. Liu, P. Nath and G. Peim, Phys. Lett. B **709**, 192 (2012) [arXiv:1111.4589]; J. L. Feng, Ann. Rev. Nucl. Part. Sci. **63** (2013) 351-382, [arXiv:1302.6587]; H. Baer, V. Barger, M. Padeffke-Kirkland and X. Tata, Phys. Rev. D **89** (2014) 037701, [arXiv:1311.4587]; H. Baer, V. Barger, D. Mickelson and M. Padeffke-Kirkland, [arXiv:1404.2277]; A. Mustafayev and X. Tata, [arXiv:1404.1386].
- [40] C. Boehm, P. S. B. Dev, A. Mazumdar and E. Pukartas, JHEP **1306**, 113 (2013) [arXiv:1303.5386 [hep-ph]]; M. W. Cahill-Rowley, J. L. Hewett, A. Ismail and T. G. Rizzo, Phys. Rev. D **86**, 075015 (2012) [arXiv:1206.5800 [hep-ph]]; C. F. Berger, J. S. Gainer, J. L. Hewett and T. G. Rizzo, JHEP **0902**, 023 (2009) [arXiv:0812.0980 [hep-ph]].
- [41] L. Roszkowski, E. M. Sessolo and A. J. Williams, JHEP **1408**, 067 (2014) [arXiv:1405.4289 [hep-ph]].
- [42] M. Cahill-Rowley, R. Cotta, A. Drlica-Wagner, S. Funk, J. Hewett, A. Ismail, T. Rizzo and M. Wood, arXiv:1405.6716 [hep-ph].
- [43] M. Bobrowski, G. Chalons, W. G. Hollik and U. Nierste, Phys. Rev. D **90**, 035025 (2014) [arXiv:1407.2814 [hep-ph]].
- [44] G. Degrandi, S. Heinemeyer, W. Hollik, P. Slavich and G. Weiglein, Eur. Phys. J. C **28**, 133 (2003) [hep-ph/0212020]; B. C. Allanach, A. Djouadi, J. L. Kneur, W. Porod and P. Slavich, JHEP **0409**, 044 (2004) [hep-ph/0406166]; S. P. Martin, Phys. Rev. D **75**, 055005 (2007) [hep-ph/0701051]; R. V. Harlander, P. Kant, L. Mihaila and M. Steinhauser, Phys. Rev. Lett. **100**, 191602 (2008) [Phys. Rev. Lett. **101**, 039901 (2008)] [arXiv:0803.0672 [hep-ph]]; S. Heinemeyer, O. Stal and G. Weiglein, Phys. Lett. B **710**, 201 (2012) [arXiv:1112.3026 [hep-ph]]; A. Arbey, M. Battaglia, A. Djouadi and F. Mahmoudi, JHEP **1209**, 107 (2012) [arXiv:1207.1348 [hep-ph]].
- [45] S. Alekhin, A. Djouadi and S. Moch, Phys. Lett. B **716**, 214 (2012) [arXiv:1207.0980 [hep-ph]].
- [46] M. Chakraborti, U. Chattopadhyay and R. M. Godbole, Phys. Rev. D **87**, no. 3, 035022 (2013) [arXiv:1211.1549 [hep-ph]].
- [47] Y. Amhis *et al.* [Heavy Flavor Averaging Group Collaboration], arXiv:1207.1158 [hep-ex].
- [48] S. Chatrchyan *et al.* [CMS Collaboration], Phys. Rev. Lett. **111**, 101804 (2013) [arXiv:1307.5025 [hep-ex]].

- [49] R. Aaij *et al.* [LHCb Collaboration], Phys. Rev. Lett. **111**, 101805 (2013) [arXiv:1307.5024 [hep-ex]].
- [50] CMS and LHCb Collaborations [CMS and LHCb Collaboration], CMS-PAS-BPH-13-007.
- [51] F. Mahmoudi, Comput. Phys. Commun. **178**, 745 (2008) [arXiv:0710.2067 [hep-ph]]. We have used version 3.3
- [52] A. Djouadi, J. -L. Kneur and G. Moultaka, Comput. Phys. Commun. **176**, 426 (2007) [hep-ph/0211331]. We have used version 2.43.
- [53] W. Altmannshofer, M. Carena, N. R. Shah and F. Yu, JHEP **1301**, 160 (2013) [arXiv:1211.1976 [hep-ph]].
- [54] B. Bhattacharjee, M. Chakraborti, A. Chakraborty, U. Chattopadhyay, D. Das and D. K. Ghosh, Phys. Rev. D **88**, no. 3, 035011 (2013) [arXiv:1305.4020 [hep-ph]].
- [55] G. Hinshaw *et al.* [WMAP Collaboration], Astrophys. J. Suppl. **208**, 19 (2013) [arXiv:1212.5226 [astro-ph.CO]].
- [56] P. A. R. Ade *et al.* [Planck Collaboration], Astron. Astrophys. (2014) [arXiv:1303.5076 [astro-ph.CO]].
- [57] G. Aad *et al.* [ ATLAS Collaboration], arXiv:1405.7875 [hep-ex].
- [58] J. Edsjo and P. Gondolo, Phys. Rev. D **56**, 1879 (1997) [hep-ph/9704361].
- [59] P. Gondolo and G. Gelmini, Nucl. Phys. B **360**, 145 (1991).
- [60] D. S. Akerib *et al.* [LUX Collaboration], Phys. Rev. Lett. **112**, 091303 (2014) [arXiv:1310.8214 [astro-ph.CO]].
- [61] G. Belanger, F. Boudjema, A. Pukhov and A. Semenov, Comput. Phys. Commun. **176**, 367 (2007) [hep-ph/0607059]; G. Belanger, F. Boudjema, A. Pukhov and A. Semenov, Comput. Phys. Commun. **177**, 894 (2007); G. Belanger, F. Boudjema, A. Pukhov and A. Semenov, Comput. Phys. Commun. **180**, 747 (2009) [arXiv:0803.2360 [hep-ph]]; G. Belanger, F. Boudjema, P. Brun, A. Pukhov, S. Rosier-Lees, P. Salati and A. Semenov, Comput. Phys. Commun. **182**, 842 (2011) [arXiv:1004.1092 [hep-ph]]; G. Belanger, F. Boudjema, A. Pukhov and A. Semenov, Comput. Phys. Commun. **185**, 960 (2014) [arXiv:1305.0237 [hep-ph]]. We have used version 3.6.7.
- [62] D. Pierce and A. Papadopoulos, Phys. Rev. D **50**, 565 (1994) [hep-ph/9312248].
- [63] A. B. Lahanas, K. Tamvakis and N. D. Tracas, Phys. Lett. B **324**, 387 (1994) [hep-ph/9312251].
- [64] A. Chatterjee, M. Drees and S. Kulkarni, Phys. Rev. D **86**, 105025 (2012) [arXiv:1209.2328 [hep-ph]].
- [65] P. Grothaus, M. Lindner and Y. Takanishi, JHEP **1307**, 094 (2013) [arXiv:1207.4434 [hep-ph]].
- [66] J. Hisano, S. Matsumoto, M. M. Nojiri and O. Saito, Phys. Rev. D **71**, 015007 (2005) [hep-ph/0407168].
- [67] H. Baer, T. Krupovnickas, A. Mustafayev, E. -K. Park, S. Profumo and X. Tata, JHEP **0512**, 011 (2005) [hep-ph/0511034].
- [68] E. Aprile [XENON1T Collaboration], Springer Proc. Phys. **148**, 93 (2013) [arXiv:1206.6288 [astro-ph.IM]].
- [69] U. Haisch and F. Mahmoudi, JHEP **1301**, 061 (2013) [arXiv:1210.7806 [hep-ph]].

- [70] For discussion on  $\text{Br}(B_s \rightarrow \mu^+ \mu^-)$  a partial list is as follows: D. Feldman, Z. Liu and P. Nath, Phys. Rev. D **81**, 117701 (2010) [arXiv:1003.0437 [hep-ph]]; S. Akula, D. Feldman, P. Nath and G. Peim, Phys. Rev. D **84**, 115011 (2011) [arXiv:1107.3535 [hep-ph]].
- [71] For further discussion on  $\text{Br}(B \rightarrow X_s \gamma)$  a partial list is as follows: U. Chattopadhyay and P. Nath, Phys. Rev. D **65**, 075009 (2002) [hep-ph/0110341]; N. Chen, D. Feldman, Z. Liu and P. Nath, Phys. Lett. B **685**, 174 (2010) [arXiv:0911.0217 [hep-ph]]; M. E. Gomez, T. Ibrahim, P. Nath and S. Skadhauge, Phys. Rev. D **74**, 015015 (2006) [hep-ph/0601163].
- [72] F. Jegerlehner and A. Nyffeler, Phys. Rept. **477**, 1 (2009) [arXiv:0902.3360 [hep-ph]].
- [73] J. L. Lopez, D. V. Nanopoulos and X. Wang, Phys. Rev. D **49**, 366 (1994) [hep-ph/9308336]; U. Chattopadhyay and P. Nath, Phys. Rev. D **53**, 1648 (1996) [hep-ph/9507386]; T. Moroi, Phys. Rev. D **53**, 6565 (1996) [Erratum-ibid. D **56**, 4424 (1997)] [hep-ph/9512396]; S. Heinemeyer, D. Stockinger and G. Weiglein, Nucl. Phys. B **690**, 62 (2004) [hep-ph/0312264]; G. -C. Cho, K. Hagiwara, Y. Matsumoto and D. Nomura, JHEP **1111**, 068 (2011) [arXiv:1104.1769 [hep-ph]].
- [74] M. Endo, K. Hamaguchi, T. Kitahara and T. Yoshinaga, JHEP **1311**, 013 (2013) [arXiv:1309.3065 [hep-ph]]; M. Endo, K. Hamaguchi, S. Iwamoto and T. Yoshinaga, JHEP **1401**, 123 (2014) [arXiv:1303.4256 [hep-ph]]; M. Chakraborti, U. Chattopadhyay, A. Choudhury, A. Datta and S. Poddar, JHEP **1407**, 019 (2014) [arXiv:1404.4841 [hep-ph]].
- [75] G. W. Bennett *et al.* [Muon G-2 Collaboration], Phys. Rev. D **73**, 072003 (2006) [hep-ex/0602035].
- [76] B. L. Roberts, Chin. Phys. C **34**, 741 (2010) [arXiv:1001.2898 [hep-ex]].
- [77] K. Hagiwara, R. Liao, A. D. Martin, D. Nomura and T. Teubner, J. Phys. G **38**, 085003 (2011) [arXiv:1105.3149 [hep-ph]].
- [78] A. Nyffeler, Nuovo Cim. C **037**, no. 02, 173 (2014) [arXiv:1312.4804 [hep-ph]].